

Unsplit Spreading: An Overlooked Signature of Long-Range Interaction

Jian-Feng Wu,^{1,2} Yi Huang,^{1,2} and Yu-Xiang Zhang^{1,2,*}

¹*Institute of Physics, Chinese Academy of Sciences, Beijing 100190, China*

²*School of Physical Sciences, University of Chinese Academy of Sciences, Beijing 100049, China*

(Dated: January 23, 2026)

In conventional lattice models, the dispersion relation $\omega(k)$ is assumed to be a smooth function. We prove that this smoothness implies the splitting of an initially localized excitation into counter-propagating wave packets. Consequently, unsplit spreading can occur only when $\omega(k)$ develops singular features, precisely what long-range interactions enable. Remarkably, this phenomenon was clearly visible in published quantum simulation experiments as early as 2014, yet it has remained unrecognized or discussed as a distinct physical effect. We show that unsplit spreading emerges in realistic open quantum systems, such as 1D and 2D subwavelength atomic arrays, where the long-lived subradiant states host effective dispersion with the required singularities. Our work establishes unsplit spreading as an experimentally accessible, smoking-gun signature of singular band structure induced by long-range physics.

A persistent research theme in the field of long-range interactions revolves around delineating the differences between a short-range model and its long-range counterpart with interactions decaying as $1/r^\alpha$, where r denotes distance and α is a positive constant [1–8]. Even at the single-particle free Hamiltonian level, the short- and long-range models differ fundamentally. As shown in Ref. [9], in the regime of *strong long-range interactions* [1] where $\alpha < d$ (with d the spatial dimension), the dispersion relation $\omega(k)$ develops a point spectrum, i.e., $\omega(k)$ consists of discrete eigenvalues rather than forming continuous bands. It underlies several anomalous phenomena: The absence of equilibration [10], the persistence of finite Poincaré recurrence times [9], etc. To go beyond the regime of $\alpha < d$, we observe that for $\alpha \geq d$, the dispersion relations may still exhibit singularities, unlike the smooth dispersion characteristic of short-range interactions. This sharp dichotomy motivates us to ask: What dynamical phenomena are strictly forbidden by the smoothness of the dispersion relation, regardless of any detail about the lattice Hamiltonian?

We find a conceptually simple answer. Suppose we generate a local excitation at a single site of a one-dimensional (1D) lattice. The excitation evolves into a time-dependent waveform. While Lieb-Robinson bound captures how fast the wavefront propagates [11–16], we focus on the overall shape of the waveform. As illustrated in Fig. 1, two distinct dynamical patterns may arise: (a) *two-packet splitting*, where the excitation separates into two counter-propagating wave packets; and (b) *unsplit spreading*, where the waveform broadens without splitting. Pattern (b) resembles the textbook behavior of Gaussian wave-packet spreading, yet we find it impossible in a lattice whenever the band dispersion relation $\omega(k)$ is smooth. This no-go theorem admits a topological interpretation, and we generalize it to 2D lattices using the Gauss–Bonnet theorem. Therefore, splitting or not is an observable for non-smooth $\omega(k)$ established by the long-range interactions. Indeed, although not noted ex-

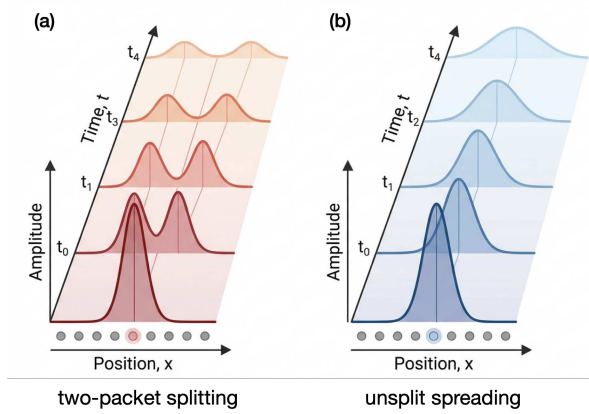


Figure 1. An initially localized excitation on a lattice exhibits two distinct diffusion behaviors: (a) it splits into two broadening wave packets that propagate in opposite directions; (b) it spreads without splitting. The solid curves represent the envelopes of the waveforms. As we will demonstrate, behavior (b) is a signature of singularities in the system’s dispersion relation arising from long-range interactions.

plicitly, we identify pattern (b) in Fig. 4(c) of Ref. [17], where 1D long-range XY model with $\alpha \approx 0.75$ is simulated using trapped ions.

This study is also motivated by a paradoxical observation regarding subradiance, an effect of quantum optics in which atomic spontaneous emission is collectively suppressed [18–23]. Although the light-mediated long-range interaction is the underlying physical mechanism [24–26], short-range toy models can nonetheless reproduce its key quantitative features [27–29], such as the power-law scaling of subradiant decay rates [30–33] and the anti-symmetric wavefunction of multiply-excited subradiant states [31, 32]. The reason is that understanding these features requires only local knowledge of $\omega(k)$ near specific k -points, which short-range models can accurately reproduce [27–29]. It suggests that the boundary between long- and short-range interactions is often blurred, particularly in light of the recent observation in Ref. [2].

This immediately raises the question of what features of $\omega(k)$ are inaccessible to short-range models and what their observable consequences are. As a reply to this question, we numerically demonstrate the presence of unsplit spreading in 1D and 2D subwavelength atom arrays [34–39].

No-go theorem for unsplit spreading. We assume the lattice dispersion relation $\omega(k)$ is twice continuously differentiable (i.e., \mathcal{C}^2), so that its first and second derivatives are continuous. The wavefunction of an excitation initialized at the site $x = 0$ reads

$$\psi(x, t) = \int_{-\pi}^{\pi} \frac{dk}{2\pi} e^{-i\omega(k)t+ikx}, \quad (1)$$

where the normalization is omitted. To evaluate Eq. (1), for given coordinate x and time t , we follow the standard stationary-phase approximation and find the Bloch waves whose group velocity v_g equals x/t :

$$v_g(k) \equiv \partial_k \omega(k) = x/t. \quad (2)$$

Equation (2) may admit multiple solutions, which we denote by \tilde{k}_i , indexed by i . Around each \tilde{k}_i , we expand $\omega(k)$ to the second order and obtain

$$\begin{aligned} \psi(x, t) &\approx \int_{-\pi}^{\pi} \frac{dk}{2\pi} \sum_i e^{-it[\omega(\tilde{k}_i) + \frac{1}{2}\partial_k^2\omega(\tilde{k}_i)(k-\tilde{k}_i)^2]} \\ &\approx \frac{1}{2\sqrt{\pi}} \sum_i e^{-i\omega(\tilde{k}_i)t} [t\partial_k^2\omega(\tilde{k}_i)]^{-1/2}, \end{aligned} \quad (3)$$

where to obtain (3) we have extended the integral to the whole real axis. Although this is not quantitatively accurate (see the Supplemental Material [40] for a comparison with exact results), it clearly reveals the dependence on $\partial_k^2\omega(k)$. This is physically meaningful because $1/|\partial_k^2\omega(k)|$ is proportional to the density of Bloch states sharing the same group velocity. Consequently, regions where $|\partial_k^2\omega(k)|$ is small tend to exhibit enhanced wavefunction amplitudes, especially when $\partial_k^2\omega(k) = 0$. To locate these peaks, we first solve the equation

$$\partial_k^2\omega(k) = 0. \quad (4)$$

Denoting its solutions by k_i^* , the corresponding peak positions are approximately $x_i(t) = v_g(k_i^*)t$.

The number of such peaks and their motions thus determine the overall shape of the wavefunction. Since $\omega(k)$ and its first two derivatives are continuous and periodic over the first Brillouin zone, we have

$$\int_{-\pi}^{\pi} \frac{dk}{2\pi} \partial_k^n \omega(k) = 0, \quad \text{for } n = 1, 2. \quad (5)$$

We ignore the case of flat bands. If $\partial_k^2\omega(k) > 0$ is positive at some point, the condition (5) with $n = 2$ implies it must take negative values elsewhere. Combined with

periodicity, which requires $\partial_k^2\omega(k)$ to return to its initial value after a full period, it is apparent that $\partial_k^2\omega(k)$ crosses zero an even number of times, generally at least twice. Each zero-crossing point corresponds to a pronounced peak of the waveform. By definition, k_i^* is where the group velocity obtains extremum. These extrema must take both positive and negative values due to the continuity and periodicity of $v_g(k)$. These correspond to right-moving and left-moving wave packets, respectively, giving rise to the split profile illustrated in Fig. 1(a).

To summarize, “unsplit spreading” is ruled out by mere smoothness and periodicity of $\omega(k)$. The most crucial step is that $\partial_k^2\omega(k)$ has at least two zeros. This is actually a topological feature of smooth functions on 1D circle (S^1). Although elementary mathematics is sufficient for 1D, we find topological viewpoint essential for 2D, where we need to consider the zeros of the determinant of Hessian $\mathcal{H}_{ij}(\vec{k}) \equiv \partial_{k_i} \partial_{k_j} \omega(\vec{k})$.

Given a non-flat dispersion, the graph $\Sigma = \{(\vec{k}, \omega(\vec{k}))\}$ defines a smooth surface in \mathbb{R}^3 generally diffeomorphic to the 2D torus T^2 . The Gauss–Bonnet theorem specified on Σ reads

$$\frac{1}{2\pi} \int_{\Sigma} K(\vec{k}) dA = \chi(T^2) = 0, \quad (6)$$

where $K(\vec{k}) = \det(\mathcal{H})/(1 + |\vec{v}_g|^2)^2$ is the Gaussian curvature, $\vec{v}_g(\vec{k}) = \nabla \omega(\vec{k})$ is the 2D group velocity, and $dA = \sqrt{1 + |\vec{v}_g|^2} d^2k$ is the induced area element on Σ . Because the weight $(1 + |\vec{v}_g|^2)^{-3/2}$ is strictly positive, the vanishing integral forces $\det(\mathcal{H})$ to take both positive and negative values across the first Brillouin zone. Consequently, the zero set $\det(\mathcal{H}) = 0$ forms a 1D sub-manifold \mathcal{S} (generically a collection of closed circles), separating regions of $\det(\mathcal{H}) > 0$ and $\det(\mathcal{H}) < 0$. Circles in \mathcal{S} plays the same role of isolated points satisfying $\partial_k^2\omega = 0$ in 1D. Along one circle in \mathcal{S} , one eigenvalue of the Hessian vanishes, while the other, denoted $\lambda(\vec{k})$, generally remains finite and influences the wavefunction amplitude. Since both $\vec{v}_g(\vec{k})$ and $\lambda(\vec{k})$ are smooth and periodic when restricted to \mathcal{S} , they generically lead to split spreading.

1D power-law interactions. To circumvent the 1D version of our no-go theorem, which requires $\omega(k)$ to belong to $\mathcal{C}^2(S^1)$, we can only violate the assumption of smoothness. Here we consider the standard models with power-law tunneling amplitudes $1/r^\alpha$. The corresponding dispersion relation reads

$$\omega_\alpha(k) = \sum_{r=1}^{\infty} \frac{2}{r^\alpha} \cos(kr). \quad (7)$$

For its derivatives, the differentiation ∂_k and infinite summation do not commute in general. Nevertheless, we may first differentiate the summand term by term and then examine the convergence of the resulting series. It turns out that $\omega_\alpha(k) \notin \mathcal{C}^k(S^1)$ if $\alpha \leq k + 1$. Thus, the cases

of $\alpha = 1, 2$ and 3 mark the threshold for $\omega_\alpha(k)$, $\partial_k \omega_\alpha(k)$, and $\partial_k^2 \omega_\alpha(k)$ to be discontinuous, respectively. In the following, we discuss them one by one.

The case of $\alpha = 1$. This is the borderline case where $\omega_1(k)$ is not continuous. The series (7) with $\alpha=1$ can be obtained by substituting $z=e^{ik}$ into the Taylor expansion of $F(z) = -\ln(1-z) - \ln(1-1/z)$ around $z = 0$. $F(z)$ has a pole at $z = 1$, hence, $\omega_1(k)$ diverges at $k = 0$. The first two derivatives are

$$\begin{aligned}\partial_k \omega_1(k) &= -\cot(k/2), \\ \partial_k^2 \omega_1(k) &= -1/[2 \sin^2(k/2)]\end{aligned}\quad (8)$$

Notably, $\partial_k^2 \omega_1(k) < 0$ (except for $k = 0$) and its magnitude obtain a unique minimum at $k = \pi$. According to Eq. (3), the waveform does not split. This is confirmed by the waveform evolution shown in Fig. 2(a).

The case of $\alpha = 2$. This is the threshold at which $\omega_\alpha(k)$ remains continuous but ceases to be differentiable, i.e., $\omega_2(k) \notin \mathcal{C}^1(S^1)$. It is convenient to express $\omega_2(k)$ on the interval $[0, 2\pi]$, where one finds $\omega_2(k) = (3k^2 - 6\pi k + 2\pi^2)/12$. Transforming back to $[-\pi, \pi]$, the derivatives read

$$\begin{aligned}\partial_k \omega_2(k) &= \begin{cases} k + \pi, & -\pi \leq k < 0; \\ k - \pi, & 0 < k \leq \pi. \end{cases} \\ \partial_k^2 \omega_2(k) &= 1, \quad k \neq 0.\end{aligned}\quad (9)$$

Thus, $\partial_k^2 \omega_2(k)$ is a constant almost everywhere except for $k = 0$, where it is undefined due to the cusp in $\partial_k \omega_2(k)$. Now Eq. (3) suggests no obvious peaks. As shown in Fig. 2(b), we observe an expanding rugged plateau, where the oscillations on top of the plateau come from the interference caused by the phase factors of Eq. (3). We classify this profile as unsplit spreading.

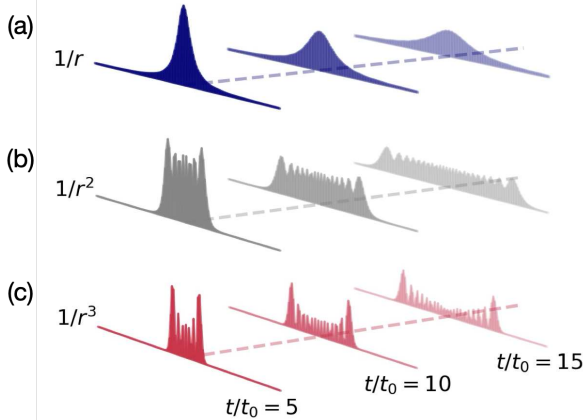


Figure 2. Spreading of waveforms under long-range interactions decaying as $1/r^\alpha$, with (a)–(c) corresponding to $\alpha = 1, 2$ and 3 , respectively. For each case, the waveforms at three different times are shown. Time is measured in units of $t_0 = a^\alpha$ where a is the lattice constant.

The case of $\alpha = 3$. This is the threshold at which $\omega_3(k) \notin \mathcal{C}^2(S^1)$. We find $\partial_k^2 \omega_3(k) = \ln[4 \sin^2(k/2)]$, which diverges at $k = 0$. Despite this singularity, the band structure now supports two-packet splitting, as shown in Fig. 2(c). This is because $\partial_k^2 \omega_3(k) = 0$ has two solutions at $k = \pm 2\pi/3$. By parity symmetry, $\omega_3(k) = \omega_3(-k)$, the group velocities at $k = \pm 2\pi/3$ have opposite signs, implying two counter-propagating sub-packets. Notably, each sub-packet contains a train of subsidiary peaks. This is typical for short-range models and is explained in the Supplemental Material [40].

Light-mediated interaction. Now we turn to the light-mediated long-range interactions in 1D and 2D *subwavelength* atom arrays, where the lattice constant, denoted by a , is shorter than resonant photon's wavelength. Before presenting the details, we note that in this system, band singularities will divide the Brillouin zone into a dissipative sector and a coherent sector (subradiant states). The latter, characterized by long lifetimes even in finite systems, effectively implementing a post-selection from which unsplit spreading could be seen. This offers a distinct pathway to circumvent the no-go theorem through open-system dynamics.

The light-mediated interaction is specified by the dyadic Green's tensor of Maxwell's equations with the corresponding boundary conditions (can be engineered by photonic structures [41–45]). We assume translation symmetry and denote the dyadic tensor by $\mathbf{G}(\mathbf{r}, \omega)$ with \mathbf{r} and ω the coordinate and frequency augments, respectively. Suppose the atoms have an excited state $|e\rangle$ and a ground state $|g\rangle$. Two atoms can interact by exchanging photons through the $|e\rangle - |g\rangle$ transition. In the Markov regime where the short-time dynamics [46] and the retardation effects can be ignored [47], the light-mediated interaction is described by an effective atomic Hamiltonian $H = H_0 + H_{\text{eff}}$. Therein, the free Hamiltonian H_0 reads $\sum_{i=1}^N (\omega_A - i\gamma_A/2) \sigma_i^\dagger \sigma_i$, where ω_A and γ_A are transition frequency and decay rate, respectively, of a single atom. The spin operators are defined by $\sigma^\dagger = |e\rangle \langle g|$ and $\sigma = |g\rangle \langle e|$. The interaction Hamiltonian is non-Hermitian [24–26]:

$$H_{\text{eff}} = -\mu_0 \omega_A^2 \sum_{i \neq j} \mathbf{d}_i^* \cdot \mathbf{G}(\mathbf{r}_i - \mathbf{r}_j, \omega_A) \cdot \mathbf{d}_j \sigma_i^\dagger \sigma_j, \quad (10)$$

where μ_0 is the vacuum permeability, \mathbf{r}_i and \mathbf{d}_i denote the position and transition dipole of each atom, respectively. Below we consider 1D atomic chains coupled to either 1D waveguide or free space, as well as 2D subwavelength atom arrays in free space.

Waveguide QED. An ideal 1D waveguide mediates an “infinite”-range Hamiltonian [48–50]

$$H_{\text{wg}} = -i \frac{\gamma_A}{2} \sum_{i \neq j} e^{-ik_A |\mathbf{r}_i - \mathbf{r}_j|} \sigma_i^\dagger \sigma_j, \quad (11)$$

where $k_A = \omega_A/c$ and c is the speed of light. As an non-Hermitian Hamiltonian, the corresponding dispersion re-

lation is complex-valued. The real part reads $\Re\omega_{\text{wg}}(k) = (\gamma_A/4) \sum_{\varepsilon=\pm 1} \cot[(k_A + \varepsilon k)a/2]$ [27], and the imaginary part reads $\Im\omega_{\text{wg}}(k) = -i\gamma_A/(4a) \sum_{\varepsilon=\pm 1} \delta(k + \varepsilon k_A)$. It is not a coincidence that $\Re\omega_{\text{wg}}$ and $\Im\omega_{\text{wg}}$ are singular at the same locations, because they are connected by the Kramers-Kronig relation.

In Fig. 3(a), the left panel shows $\partial_k^2 \Re\omega_{\text{wg}}(k)$ (see the plots of $\omega_{\text{wg}}(k)$ in the Supplemental Material [40]). We observe two continuous branches separated by the singular points $\pm k_A$, and each exhibits a nonzero minimum in absolute value. Although such double minima signal splitting waveforms for $\omega(k) \in \mathcal{C}^2(S^1)$, here the group velocity vanishes at both extrema. Consequently, no spatial splitting occurs, as confirmed by the three snapshots of

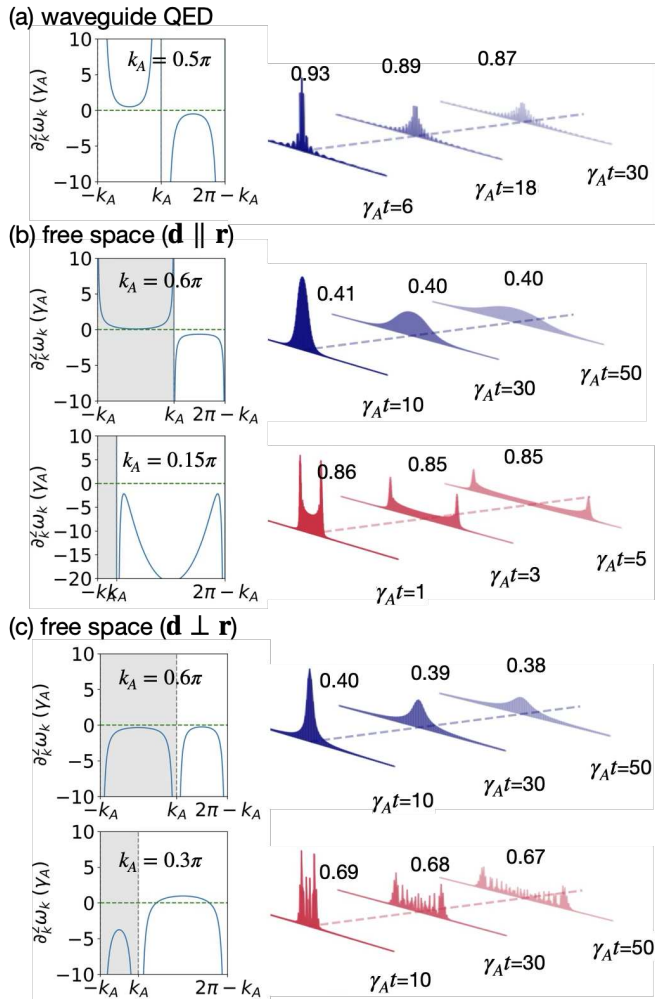


Figure 3. Left panels: $\partial_k^2 \Re\omega(k)$, the second derivative of the real part of the dispersion relation. Right panels: snapshots of the waveform of an atomic excitation initialized at the center of a chain of 751 atoms. Panels (a)–(c) correspond to (a) waveguide QED and (b, c) free space, with atomic dipole \mathbf{d} polarized parallel and perpendicular to the chain, respectively. The first Brillouin Zone is shifted to $[-k_A, 2\pi - k_A]$ for visual convenience. The probability that the excitation survives decaying is indicated near each snapshot.

the waveform at in the right panel of Fig. 3(a). Parameters used in simulation are introduced in the caption.

Atoms in free space. The dyadic Green's tensor of free space reads

$$\begin{aligned} \mathbf{G}_{\text{fs}}(\mathbf{r}, \omega_A) = & \frac{e^{ik_A r}}{4\pi k_A^2 r^3} [(k_A^2 r^2 + ik_A r - 1)\mathbb{I}_3 \\ & + (-k_A^2 r^2 - 3ik_A r + 3)\hat{\mathbf{r}}\hat{\mathbf{r}}], \end{aligned} \quad (12)$$

where $\mathbf{r} = rr\hat{\mathbf{r}}$ and $\hat{\mathbf{r}} \cdot \hat{\mathbf{r}} = 1$, and \mathbb{I}_3 is the 3×3 identity matrix. Substituting \mathbf{G}_{fs} into Eq. (10) yields effective interactions containing $1/r^\alpha$ terms with $\alpha = 1, 2$ and 3. The conventional coherent $1/r^3$ dipole-dipole interaction is obtained in the limit of $k_A a \rightarrow 0$. Importantly, when $k_A < \pi/a$, Bloch states with $|k| > k_A$ do not match with free-space radiation modes simultaneously in both energy and momentum. This means the imaginary part of the dispersion relation, $\Im\omega_{\text{fs}}(k)$, vanishes exactly for $|k| > k_A$ (the subradiant states) [28, 31].

In Fig. 3(b) we consider atomic dipoles polarized parallel to the chain, where Eq. (12) does not contain the $1/r$ term. We choose two lattice parameters, $k_A = 0.6\pi$ and 0.15π (with $a = 1$), and plot $\partial_k^2 \Re\omega_{\text{fs}}$ in the left panels, where the unshaded region corresponds to the subradiant states. For $k_A = 0.6\pi$, the subradiant branch of $\partial_k^2 \Re\omega_{\text{fs}}(k)$ attains its unique minimum magnitude at $k = \pi$, leading to unsplit spreading depicted in the right panel. In contrast, for $k_A = 0.15\pi$, the subradiant branch of $\partial_k^2 \Re\omega_{\text{fs}}(k)$ exhibit two local minima in absolute value, resulting two-packet splitting. In Fig. 3(c) the dipoles are polarized perpendicular to the chain. Now the $1/r$ term appears in Eq. (12) but the main features remain unchanged, except that for $k_A = 0.3\pi$, a train of subsidiary peaks appears as in Fig. 2(c).

2D subwavelength atom array. Unfortunately, we do not see unsplit spreading in the standard $1/r^\alpha$ Hamiltonians on square lattices [40]. While “reverse engineering” always works, i.e., we can in principle design a singular $\omega(\vec{k})$ and then reconstruct the corresponding lattice Hamiltonian, such models are typically highly artificial. Instead, we focus on physically realizable 2D subwavelength atom arrays in free space [39]. We consider a finite square lattice atoms with size and dipole polarization specified in the caption of Fig. 4. For $k_A = 0.3\pi$ (with $a=1$), the waveform splits into multiple peaks, as shown in Fig. 4(a). In contrast, for $k_A = 1.2\pi$, the excitation only diffuses weakly and remains unsplit, as illustrated in Fig. 4(b). More plots about 2D subwavelength atom arrays, and the discussion about the consistency with the determinant of the Hessian in the Supplemental Material [40], since the analysis is much more involved in 2D due to the $1/r$ terms.

Conclusion. In summary, we have proved that unsplit wave-packet spreading is forbidden in lattices with smooth band structure, which characterizes a fundamental gap between short- and long-range interactions. This

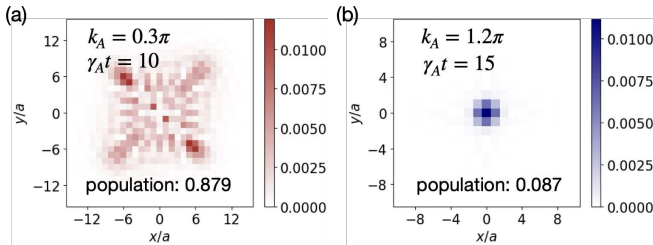


Figure 4. Waveforms of an excitation initialized in the center of a 2D square lattice (93×93) with (a) $k_A = 0.3\pi$; (b) $k_A = 1.2\pi$. The atomic dipoles are polarized along a fixed direction $\sin(\pi/12)/\sqrt{2}(\hat{x} + \hat{y}) + \cos(\pi/12)\hat{z}$, where \hat{x} and \hat{y} are unit vectors along the lattice primitive directions and \hat{z} is normal to the lattice plane. ‘Population’ refers to the survival probability of the excited state against spontaneous emission.

no-go theorem is actually a topological constraint of continuous functions on the Brillouin zone, as demonstrated using the Gauss–Bonnet theorem for 2D lattices. Long-range interactions circumvent this constraint by introducing singularities in the dispersion, enabling unsplit propagation. We also identify unsplit spreading in the subradiant states of 1D and 2D subwavelength atom arrays, which is an open-system with natural post-selection. Unsplit spreading, already present but overlooked in prior quantum simulation experiments [17], provides a direct, observable signature of singular band structure. Our work invites exploration of interacting many-body generalizations. Additional interactions are unlikely to remove the singular band structure generated by the free Hamiltonians. Then, effects such as thermalization [51, 52] and entanglement growth [6–8] in long-range interacting systems, may have features that can be traced back to singular dispersions.

Y.-X. Z. acknowledges the financial support from the Innovation Program for Quantum Science and Technology (Grant No. 2023ZD0301100), the National Natural Science Foundation of China (Grant No. 12375024), and the CAS Project for Young Scientists in Basic Research (Grant No. YSBR-100).

* ixz@iphy.ac.cn

- [1] N. Defenu, T. Donner, T. Macrì, G. Pagano, S. Ruffo, and A. Trombettoni, Long-range interacting quantum systems, *Rev. Mod. Phys.* **95**, 035002 (2023).
- [2] R. Mattes, I. Lesanovsky, and F. Carollo, Long-range interacting systems are locally noninteracting, *Phys. Rev. Lett.* **134**, 070402 (2025).
- [3] J. Eisert, M. van den Worm, S. R. Manmana, and M. Kastner, Breakdown of quasilocality in long-range quantum lattice models, *Phys. Rev. Lett.* **111**, 260401 (2013).
- [4] F. Liu, R. Lundgren, P. Titum, G. Pagano, J. Zhang, C. Monroe, and A. V. Gorshkov, Confined quasiparticle

- dynamics in long-range interacting quantum spin chains, *Phys. Rev. Lett.* **122**, 150601 (2019).
- [5] N. Defenu, D. Mukamel, and S. Ruffo, Ensemble inequivalence in long-range quantum systems, *Phys. Rev. Lett.* **133**, 050403 (2024).
- [6] T. Koffel, M. Lewenstein, and L. Tagliacozzo, Entanglement entropy for the long-range ising chain in a transverse field, *Phys. Rev. Lett.* **109**, 267203 (2012).
- [7] J. Schachenmayer, B. P. Lanyon, C. F. Roos, and A. J. Daley, Entanglement growth in quench dynamics with variable range interactions, *Phys. Rev. X* **3**, 031015 (2013).
- [8] A. Lerose and S. Pappalardi, Origin of the slow growth of entanglement entropy in long-range interacting spin systems, *Phys. Rev. Res.* **2**, 012041 (2020).
- [9] N. Defenu, Metastability and discrete spectrum of long-range systems, *Proceedings of the National Academy of Sciences* **118**, e2101785118 (2021).
- [10] M. Kastner, Diverging equilibration times in long-range quantum spin models, *Phys. Rev. Lett.* **106**, 130601 (2011).
- [11] E. H. Lieb and D. W. Robinson, The finite group velocity of quantum spin systems, *Communications in Mathematical Physics* **28**, 251 (1972).
- [12] P. Hauke and L. Tagliacozzo, Spread of correlations in long-range interacting quantum systems, *Phys. Rev. Lett.* **111**, 207202 (2013).
- [13] Z. Gong, T. Guaita, and J. I. Cirac, Long-range free fermions: Lieb-robinson bound, clustering properties, and topological phases, *Phys. Rev. Lett.* **130**, 070401 (2023).
- [14] C.-F. Chen and A. Lucas, Finite speed of quantum scrambling with long range interactions, *Phys. Rev. Lett.* **123**, 250605 (2019).
- [15] D. V. Else, F. Machado, C. Nayak, and N. Y. Yao, Improved lieb-robinson bound for many-body hamiltonians with power-law interactions, *Phys. Rev. A* **101**, 022333 (2020).
- [16] P. Richerme, Z.-X. Gong, A. Lee, C. Senko, J. Smith, M. Foss-Feig, S. Michalakis, A. V. Gorshkov, and C. Monroe, Non-local propagation of correlations in quantum systems with long-range interactions, *Nature* **511**, 198 (2014).
- [17] P. Jurcevic, B. P. Lanyon, P. Hauke, C. Hempel, P. Zoller, R. Blatt, and C. F. Roos, Quasiparticle engineering and entanglement propagation in a quantum many-body system, *Nature* **511**, 202 (2014).
- [18] R. H. Dicke, Coherence in spontaneous radiation processes, *Phys. Rev.* **93**, 99 (1954).
- [19] T. Bienaimé, N. Piovella, and R. Kaiser, Controlled dicke subradiance from a large cloud of two-level systems, *Phys. Rev. Lett.* **108**, 123602 (2012).
- [20] W. Guerin, M. O. Araújo, and R. Kaiser, Subradiance in a large cloud of cold atoms, *Phys. Rev. Lett.* **116**, 083601 (2016).
- [21] S. D. Jenkins, J. Ruostekoski, N. Papasimakis, S. Savo, and N. I. Zheludev, Many-body subradiant excitations in metamaterial arrays: Experiment and theory, *Phys. Rev. Lett.* **119**, 053901 (2017).
- [22] P. Weiss, M. O. Araújo, R. Kaiser, and W. Guerin, Subradiance and radiation trapping in cold atoms, *New Journal of Physics* **20**, 063024 (2018).
- [23] Z. Yan, J. Ho, Y.-H. Lu, S. J. Masson, A. Asenjo-Garcia, and D. M. Stamper-Kurn, Superradiant and subradiant

cavity scattering by atom arrays, *Phys. Rev. Lett.* **131**, 253603 (2023).

[24] R. H. Lehmberg, Radiation from an n -atom system. i. general formalism, *Phys. Rev. A* **2**, 883 (1970).

[25] R. H. Lehmberg, Radiation from an n -atom system. ii. spontaneous emission from a pair of atoms, *Phys. Rev. A* **2**, 889 (1970).

[26] H. T. Dung, L. Knöll, and D.-G. Welsch, Resonant dipole-dipole interaction in the presence of dispersing and absorbing surroundings, *Phys. Rev. A* **66**, 063810 (2002).

[27] Y.-X. Zhang and K. Mølmer, Theory of subradiant states of a one-dimensional two-level atom chain, *Phys. Rev. Lett.* **122**, 203605 (2019).

[28] Y.-X. Zhang and K. Mølmer, Subradiant emission from regular atomic arrays: Universal scaling of decay rates from the generalized Bloch theorem, *Phys. Rev. Lett.* **125**, 253601 (2020).

[29] Y.-X. Zhang and K. Mølmer, Free-fermion multiply excited eigenstates and their experimental signatures in 1d arrays of two-level atoms, *Phys. Rev. Lett.* **128**, 093602 (2022).

[30] T. S. Tsoi and C. K. Law, Quantum interference effects of a single photon interacting with an atomic chain inside a one-dimensional waveguide, *Phys. Rev. A* **78**, 063832 (2008).

[31] A. Asenjo-Garcia, M. Moreno-Cardoner, A. Albrecht, H. J. Kimble, and D. E. Chang, Exponential improvement in photon storage fidelities using subradiance and “selective radiance” in atomic arrays, *Phys. Rev. X* **7**, 031024 (2017).

[32] A. Albrecht, L. Henriet, A. Asenjo-Garcia, P. B. Dieterle, O. Painter, and D. E. Chang, Subradiant states of quantum bits coupled to a one-dimensional waveguide, *New J. Phys.* **21**, 025003 (2019).

[33] D. F. Kornovan, N. V. Corzo, J. Laurat, and A. S. Sheremet, Extremely subradiant states in a periodic one-dimensional atomic array, *Phys. Rev. A* **100**, 063832 (2019).

[34] G. Facchinetti, S. D. Jenkins, and J. Ruostekoski, Storing light with subradiant correlations in arrays of atoms, *Phys. Rev. Lett.* **117**, 243601 (2016).

[35] E. Shahmoon, D. S. Wild, M. D. Lukin, and S. F. Yelin, Cooperative resonances in light scattering from two-dimensional atomic arrays, *Phys. Rev. Lett.* **118**, 113601 (2017).

[36] D. Plankensteiner, C. Sommer, H. Ritsch, and C. Genes, Cavity antiresonance spectroscopy of dipole coupled subradiant arrays, *Phys. Rev. Lett.* **119**, 093601 (2017).

[37] P.-O. Guimond, A. Grankin, D. V. Vasilyev, B. Vermersch, and P. Zoller, Subradiant bell states in distant atomic arrays, *Phys. Rev. Lett.* **122**, 093601 (2019).

[38] R. Bekenstein, I. Pikovski, H. Pichler, E. Shahmoon, S. F. Yelin, and M. D. Lukin, Quantum metasurfaces with atom arrays, *Nature Physics* **16**, 676 (2020).

[39] J. Rui, D. Wei, A. Rubio-Abadal, S. Hollerith, J. Zeiher, D. M. Stamper-Kurn, C. Gross, and I. Bloch, A subradiant optical mirror formed by a single structured atomic layer, *Nature* **583**, 369 (2020).

[40] See Supplemental Material for additional discussions about 2D subwavelength atom arrays, detailed calculations and extra plots.

[41] P. Lodahl, S. Mahmoodian, and S. Stobbe, Interfacing single photons and single quantum dots with photonic nanostructures, *Rev. Mod. Phys.* **87**, 347 (2015).

[42] S.-P. Yu, J. A. Muniz, C.-L. Hung, and H. J. Kimble, Two-dimensional photonic crystals for engineering atom-light interactions, *Proceedings of the National Academy of Sciences* **116**, 12743 (2019).

[43] R. Pennetta, M. Blaha, A. Johnson, D. Lechner, P. Schneeweiss, J. Volz, and A. Rauschenbeutel, Collective radiative dynamics of an ensemble of cold atoms coupled to an optical waveguide, *Phys. Rev. Lett.* **128**, 073601 (2022).

[44] A. Tiranov, V. Angelopoulou, C. J. van Diepen, B. Schrinski, O. A. D. Sandberg, Y. Wang, L. Midolo, S. Scholz, A. D. Wieck, A. Ludwig, A. S. Sørensen, and P. Lodahl, Collective super- and subradiant dynamics between distant optical quantum emitters, *Science* **379**, 389 (2023).

[45] M. Teçer, M. Di Liberto, P. Silvi, S. Montangero, F. Romanato, and G. Calajó, Strongly interacting photons in 2d waveguide qed, *Phys. Rev. Lett.* **132**, 163602 (2024).

[46] Y.-X. Zhang, Zeno regime of collective emission: Non-markovianity beyond retardation, *Phys. Rev. Lett.* **131**, 193603 (2023).

[47] K. Sinha, P. Meystre, E. A. Goldschmidt, F. K. Fatemi, S. L. Rolston, and P. Solano, Non-markovian collective emission from macroscopically separated emitters, *Phys. Rev. Lett.* **124**, 043603 (2020).

[48] D. E. Chang, L. Jiang, A. V. Gorshkov, and H. J. Kimble, Cavity qed with atomic mirrors, *New J. Phys.* **14**, 063003 (2012).

[49] D. E. Chang, J. S. Douglas, A. González-Tudela, C.-L. Hung, and H. J. Kimble, Colloquium: Quantum matter built from nanoscopic lattices of atoms and photons, *Rev. Mod. Phys.* **90**, 031002 (2018).

[50] A. S. Sheremet, M. I. Petrov, I. V. Iorsh, A. V. Poshakinskiy, and A. N. Poddubny, Waveguide quantum electrodynamics: Collective radiance and photon-photon correlations, *Rev. Mod. Phys.* **95**, 015002 (2023).

[51] B. Neyenhuis, J. Zhang, P. Hess, J. Smith, A. Lee, P. Richerme, Z.-X. Gong, A. Gorshkov, and C. Monroe, Observation of prethermalization in long-range interacting spin chains, *Science Advances* **3** (2017).

[52] S. Sugimoto, R. Hamazaki, and M. Ueda, Eigenstate thermalization in long-range interacting systems, *Phys. Rev. Lett.* **129**, 030602 (2022).

Supplemental Material to “Unsplit Spreading: An Overlooked Signature of Long-Range Interaction”

Jian-Feng Wu,^{1, 2} Yi Huang,^{1, 2} and Yu-Xiang Zhang^{1, 2, *}

¹ Institute of Physics, Chinese Academy of Sciences, Beijing 100190, China

² School of Physical Sciences, University of Chinese Academy of Sciences, Beijing 100049, China

(Dated: January 23, 2026)

This Supplemental Material is arranged as follows. In Sec. I, we plot the dispersion relations corresponding to the second derivatives shown in Fig. 3 of the main text. In Sec. II, we benchmark the precision of the stationary-phase approximation used in Eq. (3) of the main text. In Sec. III, we present details about the calculation of 2D lattices, including the case of power-law decaying Hamiltonian and the light-mediated interactions in 2D subwavelength atom arrays.

I. DISPERSION AND DISSIPATION OF LIGHT-MEDIATED INTERACTION

In Fig. (3) of the main text, we showed only the second derivatives of the real part of the dispersion relations, $\partial_k^2 \Re \omega(k)$. Here we plot the corresponding complex-valued dispersion relations in Fig. S-1.

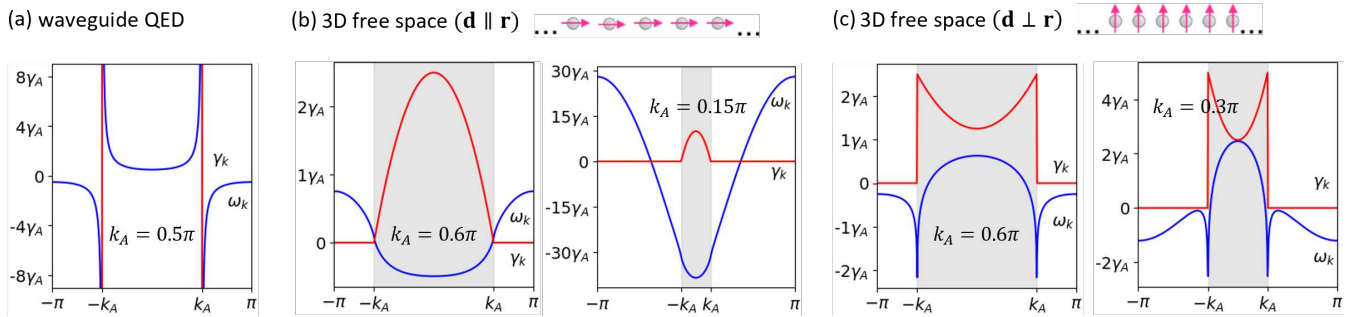


Figure S-1. Real part (blue solid curve) and imaginary part (red solid curve) of the dispersion ω_k (in units of γ_A) for the setups of (a) waveguide QED; (b,c) atoms in free space with polarization \mathbf{d} parallel and perpendicular to the chain, respectively. Values of k_A are specified in the figures. We take lattice constant $a = 1$.

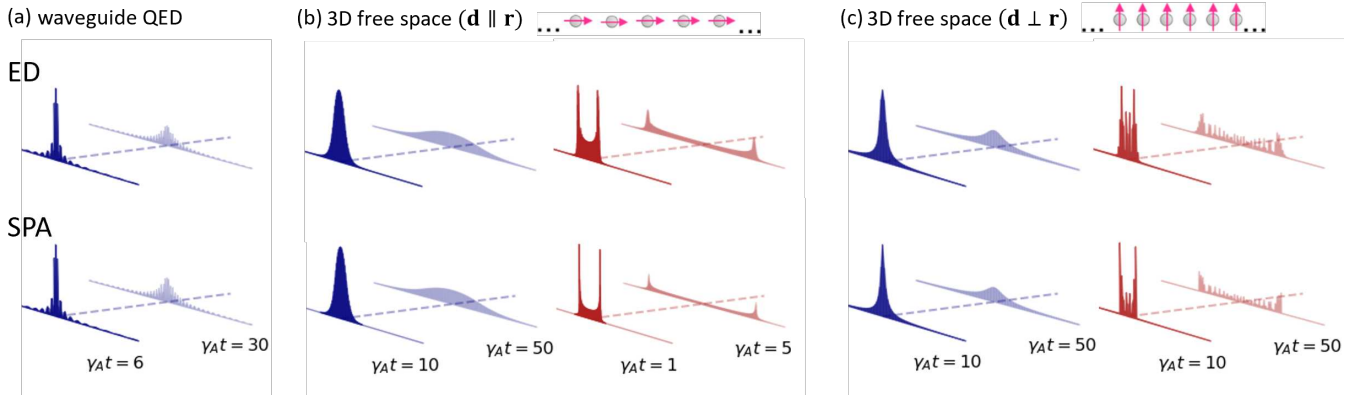


Figure S-2. Comparing exact dynamics and stationary phase approximation for the setups of (a) waveguide QED; (b,c) atoms in the 3D free space with polarization \mathbf{d} parallel and perpendicular to the chain, respectively. The waveforms of the first row are calculated from exact dynamics (ED), while the second row shows the results from stationary phase approximation (SPA). Values of k_A are the same as those in the main text.

* iyxz@iphy.ac.cn

II. BENCHMARKING THE STATIONARY-PHASE APPROXIMATION

In Eq. (3) of the main text, we have approximated $\omega(k)$ by Taylor expansion up to the 2nd order, and employed the Gaussian integral formula to associate the dominant peaks of $|\psi(x, t)|$ with the zeros of $\partial_k^2\omega(k)$, at which Eq. (3) of the main text diverges actually. Thus, this approach cannot be quantitatively precise and we need to benchmark to what extent it captures the waveforms.

We examine the stationary-phase approximation by applying it to all the examples of 1D models of light-mediated interactions studied in the main text. We apply Eq. (3) of the main text to obtain $|\psi(x, t)|^2$ and normalize it, considering that this is an open-system evolution so that the normalization should be the probability that no spontaneous emission occurs. The results are shown in the lower panels of Fig. S-2. Comparing them with exact numerical simulation depicted in the upper panels of Fig. S-2, we see that the stationary-phase approximation is not qualitatively good, but it does capture the profile.

Moreover, in Fig. 2(c) and Fig. 3(c) of the main text, we observe that the splitting waveform has a train of subsidiary peaks, in contrast to the smooth profile displayed in Fig. 3(b) of the main text. This can be understood within the formalism of stationary-phase approximation. Note that now we have zeros of $\partial_k^2\omega(k)$, as shown in the left panels of Fig. 3(c) of the main text. Around each zero point of $\partial_k^2\omega(k)$, the group velocity $v_g(k)$ is not monotonic with respect to k , which means that for a given x/t , there could be two solutions (see Fig. S-3). These two Bloch waves then interfere at $x = v_g t$, leading to the subsidiary peaks. Similar statements also apply to waveguide QED depicted in Fig. 3(a) of the main text. Therein, the interference comes from the Bloch modes belonging to different branches separated by $k = \pm k_A$.

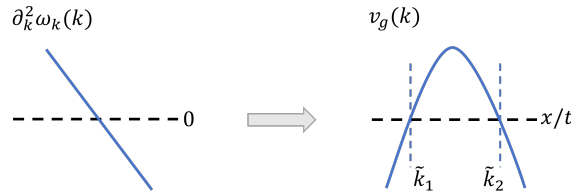


Figure S-3. Schematic plot of the origin of train of subsidiary peaks. The non-monotonic behavior of $v_g(k)$ near $\partial_k^2\omega_k(k) = 0$ shows multiple solutions of stationary points, which give rise to interference.

III. SPREADING IN 2D LATTICES

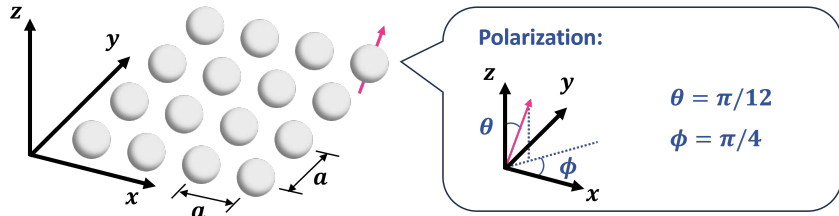


Figure S-4. 2D square lattice. Atoms are arranged in the $x - y$ plane and the polarization is parameterized by spherical coordinate (θ, ϕ) . The definitions of these angles are shown in the figure.

A. Power-law hopping ($\alpha = 2$)

Here we show the spreading of a local excitation on 2D square lattice with power-law hopping $H = \sum_{i,j} J(r_{i,j})\sigma_i^\dagger\sigma_j = \sum_{i,j} 1/r_{i,j}^\alpha \sigma_i^\dagger\sigma_j$ when $\alpha = 2$. This is the threshold where we do not have a pure point spectrum but still gain singularities in the dispersion relation.

In contrast to the corresponding 1D case where $\alpha = 1$, the waveform now splits into multiple peaks as shown in Fig. S-5. We further check the determinant of Hessian $[\mathcal{H}(\vec{k})]$ using finite differences, and find that there is a closed loop that satisfies $\det(\mathcal{H}) = 0$. As analyzed in the main text, this is where the splitting waveform results from.

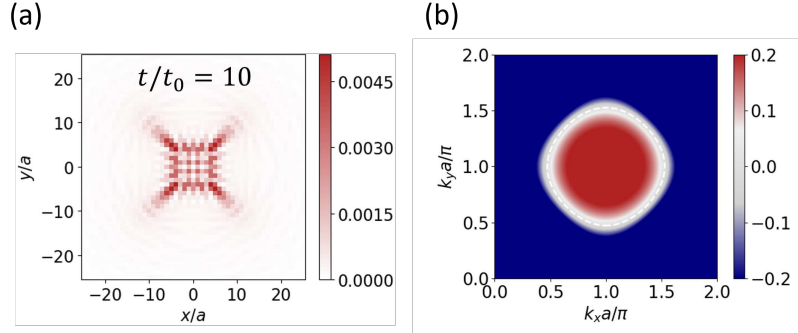


Figure S-5. Waveform and $\det(\mathcal{H})$ (in units of $1/a^6$ where a is the lattice constant) of 2D power-law model: (a) Exact dynamics on a 93×93 square lattice. Time is measured in units of $t_0 = a^2$; (b) Determinant of Hessian calculated from dispersion (the discrete Fourier transformation of $J(r_{ij})$) using finite differences. The white dashed line denotes $\det(\mathcal{H}) = 0$.

B. 2D subwavelength atom arrays

Firstly, in Fig. S-4 we illustrate the setup and the direction of the polarization of the atomic transition dipoles used in the main text.

Next, we discuss the corresponding $\det(\mathcal{H})$ of 2D subwavelength atom arrays. In the main text, we consider a finite array so that all the simulations are straightforward and meaningful. Here, however, it becomes complicated to obtain converge dispersion relation due to the presence of $1/r$ terms. As noted in the main text, it is not guaranteed that differentiation commutes with infinite summation. In the literature of quantum optics, people usually “regularize” the Hamiltonians in order to circumvent the divergence.

To proceed, we write the dispersion relation (real part) in the form of summation over reciprocal space:

$$\Re \omega_{\text{fs}}(\mathbf{k})/\gamma_A = -\frac{3\pi}{k_A} \Re \sum_{\mathbf{r}_n \neq 0} e^{i\mathbf{k} \cdot \mathbf{r}_n} \mathbf{G}_{\text{fs}}(\mathbf{r}_n, \omega_A) = -\frac{3\pi}{k_A} \Re \left(\frac{1}{a_x a_y} \sum_{\mathcal{G}} \mathbf{g}(\mathcal{G} - \mathbf{k}, \omega_A) - \mathbf{G}_{\text{fs}}(\mathbf{0}, \omega_A) \right), \quad (\text{S-1})$$

where a_x, a_y are separations along x, y axis respectively, \mathcal{G} is the reciprocal lattice vector and \mathbf{g} is defined as (differs from the definition in Ref. [1] by a sign due to the opposite sign convention for $\mathbf{G}_{\text{fs}}(\mathbf{r}, \omega_A)$)

$$\mathbf{g}_{\alpha\beta}(\mathbf{p}, \omega_A) = \int \frac{dp_z}{2\pi} \frac{1}{k_A^2} \frac{k_A^2 \delta_{\alpha\beta} - p_\alpha p_\beta}{p^2 - k_A^2}. \quad (\text{S-2})$$

Note that both parts on the right hand side diverge. Following the treatment of Ref. [1], we assume the position of each atom is not fixed in space but has a wavefunction with a finite spatial uncertainty characterized by a length scale a_{ho} . It serves as a regularization parameter with which the formula becomes

$$\Re \omega_{\text{fs}}(\mathbf{k})/\gamma_A = -\frac{3\pi}{k_A} \Re \left(e^{k_A^2 a_{\text{ho}}^2/2} \frac{1}{a_x a_y} \sum_{\mathcal{G}} \mathbf{g}^*(\mathcal{G} - \mathbf{k}, \omega_A) - \mathbf{G}_{\text{fs}}^*(\mathbf{0}, \omega_A) \right). \quad (\text{S-3})$$

The regularized \mathbf{g}^* reads

$$\begin{aligned} g_{xx}^*(\mathbf{p}, \omega_A) &= -(k_A^2 - p_x^2) \mathcal{I}_0, \\ g_{yy}^*(\mathbf{p}, \omega_A) &= -(k_A^2 - p_y^2) \mathcal{I}_0, \\ g_{zz}^*(\mathbf{p}, \omega_A) &= -(k_A^2 \mathcal{I}_0 - \mathcal{I}_2), \\ g_{xy}^*(\mathbf{p}, \omega_A) &= g_{yx}^*(\mathbf{p}, \omega_A) = p_x p_y \mathcal{I}_0, \\ g_{xz}^*(\mathbf{p}, \omega_A) &= g_{zx}^*(\mathbf{p}, \omega_A) = g_{yz}^*(\mathbf{p}, \omega_A) = g_{zy}^*(\mathbf{p}, \omega_A) = 0, \end{aligned}$$

where

$$\begin{aligned}\mathcal{I}_0(\mathbf{p}, \omega_A) &= \mathcal{C} \frac{\pi e^{-a_{\text{ho}}^2 \Lambda^2/2}}{\Lambda} \left[-i + \text{erf} \left(\frac{a_{\text{ho}} \Lambda}{\sqrt{2}} \right) \right], \\ \mathcal{I}_2(\mathbf{p}, \omega_A) &= \Lambda^2 \mathcal{I}_0 - \mathcal{C} \frac{\sqrt{2\pi}}{a_{\text{ho}}}, \\ \mathcal{C}(\mathbf{p}, \omega_A) &= \frac{1}{2\pi k_A^2} e^{-a_{\text{ho}}^2 p^2/2}, \\ \Lambda(\mathbf{p}, \omega_A) &= \sqrt{k_A^2 - p^2}.\end{aligned}$$

Following Ref. [1, 2], we set $a_{\text{ho}}/a = 0.1$ [we have examined that different choices of small a_{ho} can change the dispersions quickly, but the derivatives are relatively less sensitive to a_{ho} in regions where $\det(\mathcal{H})$ does not diverge]. and calculate the derivatives of g^* to get $\det(\mathcal{H})$. Results are shown in Fig. S-6. For $k_A = 0.3\pi$, there are closed loops of $\det(\mathcal{H}) = 0$ inside the subradiant zone, which give rise to the splitting waveforms. This is further supported by more snapshots of the waveform evolution in Fig. S-7(a).

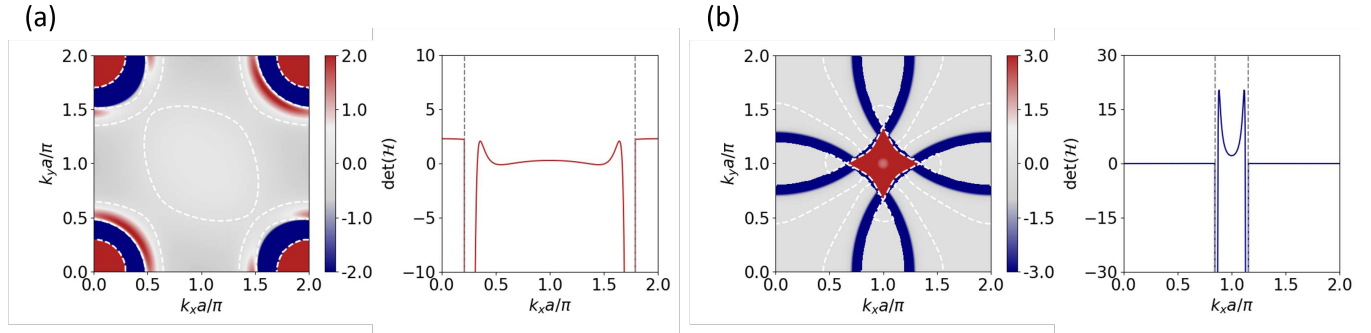


Figure S-6. $\det(\mathcal{H})$ (in units of γ_A/a^4) of 2D square lattice (93×93) models calculated from regularized dispersion ($a_{\text{ho}}/a = 0.1$) with (a) $k_A = 0.3\pi$; (b) $k_A = 1.2\pi$. Atoms arrangement and atomic polarization are the same as those in the main text. The white dashed lines on the left panels of (a)(b) denote $\det(\mathcal{H}) = 0$. On the right panels, determinants are plotted along $k_x = k_y$. Singularities at $|\vec{k}| = k_A$ are marked by grey dashed lines.

For $k_A = 1.2\pi$, while we see unsplit spreading in Fig. 4(b) of the main text, the regularized Hamiltonian still displays a loop of $\det(\mathcal{H}) = 0$ in the subradiant zone, as shown in Fig. S-6(b). However, by choosing $k_A = 1.2\pi$, this loop is adjacent to the diverging singularities at $|\vec{k}| = k_A$, which is also the boundary of the subradiant regime. This is clearly demonstrated in cross-section depicted in the right panel of Fig. S-6. It turns out that in finite systems, Bloch modes corresponding to this loop still has a significant rate of spontaneous emission, i.e., a short lifetime. We can then expect that the dynamics is dominated by the inner part of the subradiant zone, which is free from zeros of $\det(\mathcal{H})$. In Fig. S-7(b) we show more snapshots of the waveform at different times. The plots confirm unsplit spreading in this case, in contrast to the splitting waveforms displayed in Fig. S-7(a).

Moreover, we can tune the parameters of the 2D subwavelength atom arrays to see splitting in one direction, and unsplit spreading on the other direction. This is illustrated for various lattice parameters in Fig. S-8.

[1] J. Perczel, J. Borregaard, D. E. Chang, H. Pichler, S. F. Yelin, P. Zoller, and M. D. Lukin, Photonic band structure of two-dimensional atomic lattices, *Phys. Rev. A* **96**, 063801 (2017).
[2] D. Fernández-Fernández and A. González-Tudela, Tunable directional emission and collective dissipation with quantum metasurfaces, *Phys. Rev. Lett.* **128**, 113601 (2022).

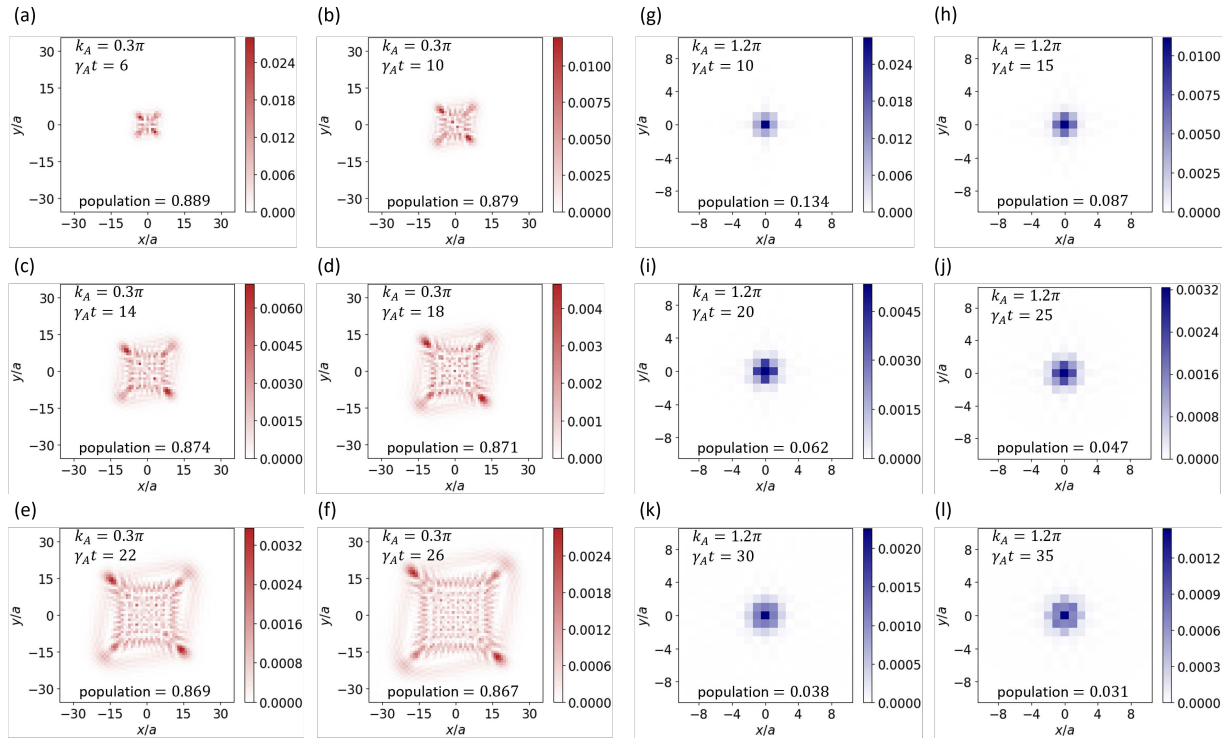


Figure S-7. Waveforms at different $\gamma_A t$ on a 2D square lattice (93×93) with (a-f) $k_A = 0.3\pi$; (g-l) $k_A = 1.2\pi$. Atoms arrangement and atomic polarization are the same as those in the main text.

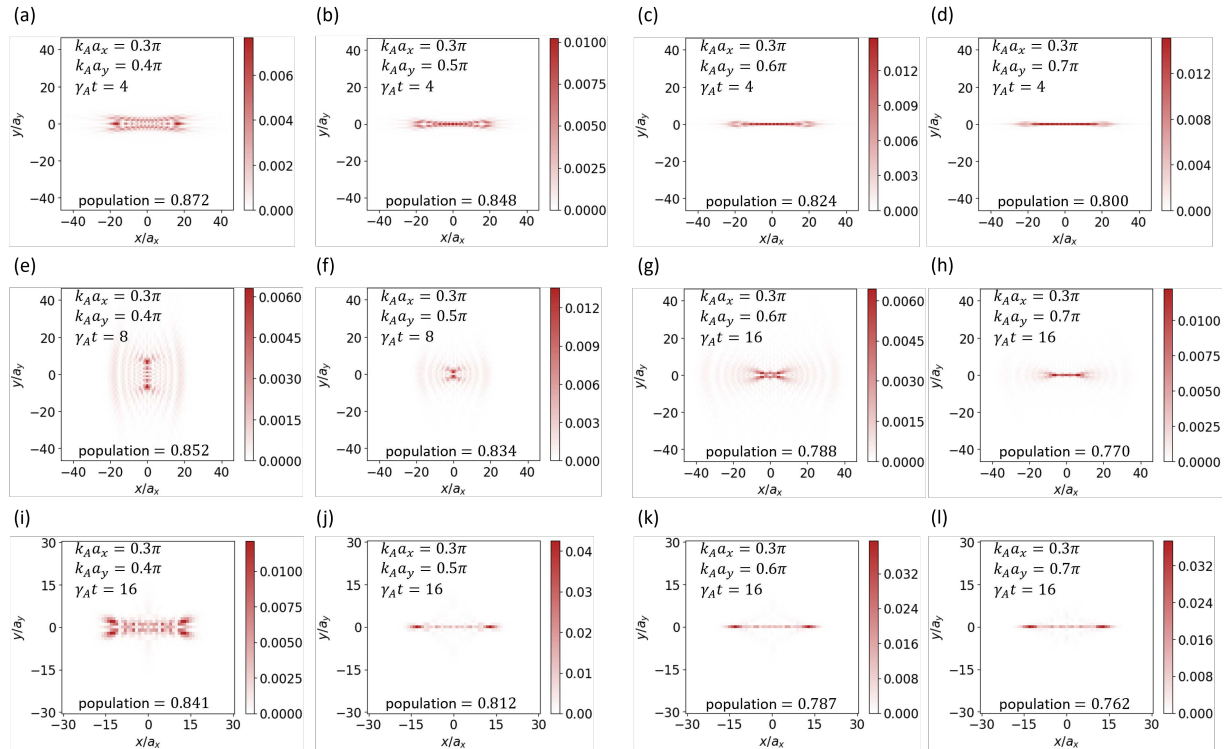


Figure S-8. Waveforms on 2D rectangular lattices (93×93) with polarization along (a-d) x axis; (e-h) y axis; (i-l) z axis.